applied optics

Dynamic projection theory for fringe projection profilometry

Hong Sheng,[1] Jing Xu,[1,*] and Song Zhang[2]

[1]State Key Laboratory of Tribology, Department of Mechanical Engineering, Tsinghua University, Beijing 100084, China
[2]School of Mechanical Engineering, Purdue University, West Lafayette, Indiana 47907, USA
*Corresponding author: jingxu@tsinghua.edu.cn

Received 17 July 2017; revised 21 September 2017; accepted 21 September 2017; posted 21 September 2017 (Doc. ID 302562); published 18 October 2017

Fringe projection profilometry (FPP) has been widely used for three-dimensional reconstruction, surface measurement, and reverse engineering. However, FPP is prone to overexposure if objects have a wide range of reflectance. In this paper, we propose a dynamic projection theory based on FPP to rapidly measure the overexposed region with an attempt to conquer this challenge. This theory modifies the projected fringe image to the next better measurement based on the feedback provided by the previously captured image intensity. Experiments demonstrated that the number of overexposed points can be drastically reduced after one or two iterations. Compared with the state-of-the-art methods, our proposed dynamic projection theory measures the overexposed region quickly and effectively and, thus, broadens the applications of FPP.

OCIS codes: (050.5080) Phase shift; (120.2830) Height measurements; (100.5088) Phase unwrapping.

https://doi.org/10.1364/AO.56.008452

1. INTRODUCTION

Three dimensional (3D) shape measurement is widely applied in industrial inspection and quality measurement [1–3]. There are numerous 3D shape measurement methods developed, such as stereovision [4,5], line laser scanning [6–8], and fringe projection profilometry (FPP) [9–11]. Compared with most other 3D measurements, FPP has the advantages of high measurement accuracy and point density [12]. Therefore, FPP has been widely used in reverse engineering, medical engineering, aviation, along with other fields. A FPP system consists of a projector, a camera, and a computer. The fringe patterns are projected onto the target object surface, the camera captures the images with the reflected patterns of deformation, the computer decodes the phase of the captured images, and, finally, a 3D shape of the object surface can be reconstructed after system calibration [13,14].

FPP, after all, is an intensity-based coding strategy and, thus, is sensitive to surface texture and reflectance [15]. Therefore, for FPP, there is still an issue when measuring complex optical objects. In this case, the surface has a large span of reflectance caused by the diversity of surface texture, color, and other optical properties. Therefore, the captured images include the high-quality fringe areas where high-quality data can be reconstructed, as well as overexposed and underexposed regions, where high-quality 3D reconstruction is difficult to be achieved. Especially, for those overexposed or underexposed regions, the camera fails to capture high-quality information about the object surface with the same projection brightness and exposure time used to capture other regions. Therefore, for objects with a large span of reflectivity, there may be different degrees of overexposure when using the traditional FPP method to measure the entire target surface.

To conquer this challenge, we propose a new dynamic projection theory for FPP. The main idea is as follows: without any additional information or operations other than the feedback provided by previously captured object surface images, the proposed method can modify the projection information dynamically to reduce the number of overexposed points. Accurate 3D surface information of the target is obtained through automatic iteration measurements that can effectively reduce overexposure points in one or two iterations. With the dynamic projection theory, FPP can measure the overexposed regions and, thus, can properly measure objects with high-reflectivity variations.

The proposed dynamic fringe projection theory includes the following process:

(1) Obtain feedback of the intensity of all pixels from captured images: For each overexposed point, there is a series of intensities, which include effective intensity information (properly exposed value) and invalid intensity information (overexposed value). The properly exposed value of the pixel point is used to estimate the theoretical value for the overexposed value; the theoretical overexposed value is used to estimate the proper value to project.

(2) Find the coordinate relationship of the projector and the overexposed pixels: Because intensity information is acquired by the camera, and the intensity of the projector image is modified, it is important to find the relationship between the projector and camera pixels. In this paper, the rank information of properly exposed points is used to estimate the projector pixel coordinates of overexposed points and obtain the relationship of the coordinates for the camera and projector.

(3) Modify the projector images and repeat the projection: After obtaining the relationship between the coordinates of the camera and the projector, new projector images can be generated based on the feedback information and projected again to get new iterations of feedback. When the number or proportion of overexposed points has been reduced to meet the requirement, the full 3D information can be decoded and reconstructed with the latest information.

This paper is organized as follows: some related research is reviewed in Section 2, and the principle is introduced in Sections 3.A and 3.B. The simulation of the phase error caused by overexposure is showed in Section 3.C. Experimental results with the dynamic projection theory are presented in Section 4. The conclusion and future work are summarized in Section 5.

2. LITERATURE REVIEW

Over the past decades, structured-light-based 3D shape measurement methods have been extensively studied due to their flexible structured pattern generation nature [16–20]. FPP is one special case of structured light method for 3D shape measurement that uses sinusoidal patterns called fringe patterns. Compared with pixel-level accuracy achieved by using binary structured patterns, FPP achieves a sub-pixel because of the use of sinusoidal fringe patterns. However, one of the problems associated with the FPP method is that the captured fringe patterns have to be sinusoidal. Thus, if a target object has a large span of reflectivity variations, overexposure or underexposure could occur, and the overexposure makes the sinusoidal pattern be non-sinusoidal due to pattern saturation, leading to measurement error.

To solve the problem associated with overexposure due to saturation, researchers have proposed numerous methods, including the pretreatment of object surface, the combination with polarized light, the requirement of multiple exposures, the use of regularization, and so on. The pretreatment method in Ref. [21] can reduce the reflectivity variation by uniformly coating the object surface with powder; yet, coating the surface is not desirable and often unpractical. In Ref. [22], using polarized light can work well to reduce problems caused by highly specular surfaces, but its effectiveness is limited if the object surface is diffuse, and properly adjusting a polarization angle is time consuming, and sometimes it is not easy. In Ref. [23], the multiple exposure method by adjusting projection brightness and camera exposure time can theoretically avoid the acquisition of overexposed points, but such a method is often not efficient due to the capture of many images. In Ref. [24], a method is proposed to extract curvilinear from overexposed images with Steger's method and perspective distortion. Although it has high precision, it only works for linear extraction and is not suitable for complex 3D objects. In Ref. [25], it can measure the shiny surfaces regardless of the saturation level, but it requires the acquisition of many patterns, slowing down the measurement process. To deal with overexposure in the captured fringe pattern image, Ref. [26] estimates the geometric sketch of the error area first and uses iterative regularization to inpaint the fringe pattern. Only a fringe pattern is projected, so it is more efficient, but it is limited by the area size with error and is difficult to apply when the overexposed area is large.

In Ref. [27], the area of interest in the captured fringe pattern image is detected, which is efficient to deal with noise and can improve the quality of reconstruction, but it is not suitable for overexposure. In Ref. [28], both the regular fringe pattern and inverted fringe patterns (i.e., with 180 phase differences) are projected and select the properly captured images for each point measurement. This method can handle overexposure problems at a certain degree, but fails if all inverted and regular patterns are saturated. In Ref. [29], two sets of gray-coded low-frequency patterns and two sets of gray-coded high-frequency patterns are combined to project on the same point for 3D reconstruction. Because the low-frequency gray-coded patterns have high resistance to sub-surface scattering, and the high-frequency gray-coded patterns have high internal reflection resistance; the combination can well reconstruct a target object with shiny areas. Since the number of projected images in this method is at least four times that of the traditional FPP, the measurement speed is drastically slowed down. In Ref. [21], an adaptive FPP using the gray code with line shifting is proposed. The intensity mask is updated and, then, is used to modify the projected patterns iteratively. Some target objects with complex reflectivity can be reconstructed well, but it requires three iterations and is time consuming. In Ref. [30], the projected pattern is transformed into diffused light with a diffuser, so that the reflected light of the specular object can be captured and then decoded. However, the position of the projector, the diffuser, and the object must be carefully designed and must adjust for different conditions, making it difficult to be reproduced by a non-expert. In Ref. [31], an adaptive fringe pattern projection method is adopted, which uses the Levenberg–Marquardt algorithm to determine the modification coefficient and adjusts the projected patterns to avoid image saturation. But, the low multiple input gray levels need to be selected carefully, and the noise of the camera and projector could affect the effectiveness of this approach. In Ref. [32], a FPP algorithm using the sparse dictionary learning and sparse coding techniques is proposed, which can improve the robustness of the system.

Most of the state-of-the-art methods for measuring overexposure areas are complex, time consuming, or insufficient for severe overexposure. Therefore, we propose a flexible and fast method for objects with highly diverse reflectivity. For higher accuracy, sinusoidal fringe patterns are adopted first. Then, an interpolation model is developed to estimate the point spread function of those overexposed points with properly exposed object points. A gray correction function is derived for overexposed points, and a gray correction mask is generated to modify the projected patterns. The intensity of an overexposed region is reduced and can be measured. Overexposure is also

a problem in other applications, such as wavefront reconstruction. Reference [33] puts forward an experimental technique to address overexposure of highly reflective surfaces for enhanced object wavefront reconstruction. It uses random phase modulation and speckle illumination to minimize the strong specular reflections. Comparing Ref. [33] with our method, both the illuminations are adjusted, but we modify the projection based on feedback, while it adjusts the illumination in advance to extend the measurement application. Compared with the state-of-the-art methods, the advantages of dynamic projection theory are as follows:

(1) The operation is simple without any pretreatment. Dynamic projection theory can automatically adjust the projected image information from the feedback image captured by the camera.

(2) There is high measurement efficiency. Only 1–2 iterations are required to decode the 3D information of the overexposed area.

(3) The measurement range is wide. Objects with a high degree of overexposure and more complex optical surfaces can be properly measured.

3. PRINCIPLE OF DYNAMIC PROJECTION THEORY

The proposed dynamic projection theory is a new method for measuring complex optical objects based on FPP. In this method, the original projector images are modified using the feedback of the object surface captured by the camera. The flow chart is shown in Fig. 1. The main steps are as follows:

(1) Use the properly exposed information to fit the approximate location of the projection pixels corresponding to the camera overexposure pixels;

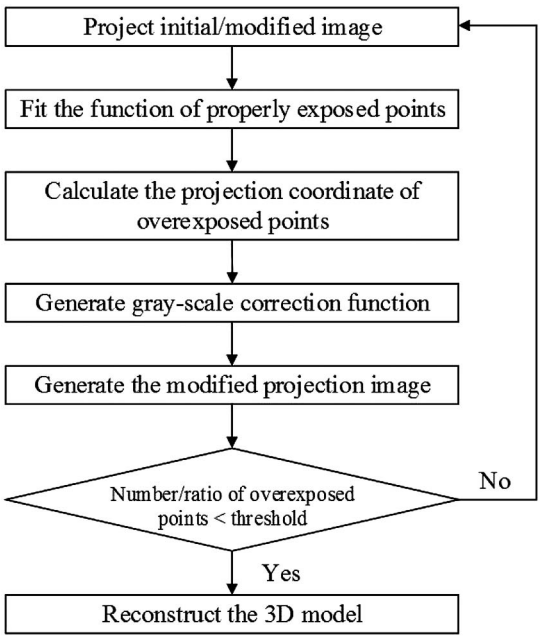

Fig. 1. Flow chart of dynamic projection theory.

(2) Use the camera overexposure information and the corresponding projection coordinate information to calculate the gray-scale correction function of the projected images;

(3) Use the gray-scale correction function to modify the projected image intensity of the overexposed area (keep the phase information unchanged and only reduce the projection intensity);

(4) Project the modified image, repeat the above steps until the number or proportion of overexposed points meet the requirement, and then reconstruct the target object.

A. Finding the Point Spread Function of the Overexposed Pixel Point

A four-step phase-shifting method is adopted for 3D measurement. To modify the corresponding projection image intensity for an overexposed point, the point spread function between the camera and projector pixel must be found. As the camera intensities of overexposed pixels are distorted, the correspondence between the camera and projector obtained through traditional FPP is incorrect and cannot be directly used. Since the intensity of the camera's properly exposed pixel (u, v) is accurate, we can calculate the point spread function $(i, j) = F(u, v)$ and determine the corresponding projection coordinate (i, j) of a properly exposed pixel with the phase-shifting method. Assuming that the target object surface is overall smooth, for each overexposed camera pixel (u_{oe}, v_{oe}), a rough corresponding area in the projection image can be obtained through interpolation and error compensation, where subscript oe represents overexposure. Especially since not the accurate corresponding pixel but a corresponding area is determined for an overexposed pixel.

The procedure of interpolation is conducted as follows: (1) Decode properly exposed pixels and extract overexposed points; (2) determine independent variable and dependent variable sequences; (3) calculate corresponding pixels with cubic spline interpolation; (4) expand corresponding pixels to square areas.

To perform the detail, the properly exposed camera pixels are first decoded, which establishes the relationship between $\{(u, v)\}$ and $\{(i, j)\}$. Then, for each overexposed pixel, for example, (u_{oe}, v_{oe}), two sequences are selected from the properly exposed pixels. As shown in Fig. 2, the sequence with the same camera pixel ordinate $\{(u_1, v_{oe}), (u_2, v_{oe}), \ldots, (u_{oe}, v_{oe}), \ldots\}$ and the sequence of their corresponding projected pattern pixel $\{(i_1, j_1), (i_2, j_2), \ldots, (i_{oe}, j_{oe}), \ldots\}$ are extracted, in which (i_{oe}, j_{oe}) is the goal to calculate. Then, the sequence $\{(u_1, i_1), (u_2, i_2), \ldots, (u_{oe}, i_{oe}), \ldots\}$ is obtained from these two sequences, and cubic spline interpolation is conducted to determine the corresponding abscissa i_{oe}. With combination of later error compensation, cubic spline interpolation is enough to roughly estimate the corresponding pixel. For the corresponding ordinate j_{oe}, a similar action is performed with the sequence of the same camera pixel abscissa.

Indeed, as there inevitably exists a deviation about the interpolation, the accurate corresponding pixels cannot be determined. So, for each overexposed camera pixel, the corresponding pixel is determined at first. Then, assuming that the maximum error is a pixels, the corresponding pixel is expanded to a square area centered on the pixel with a side length of $(2a + 1)$ pixels as the red square shown in Fig. 2. The value of a is determined by the continuity of the object surface and

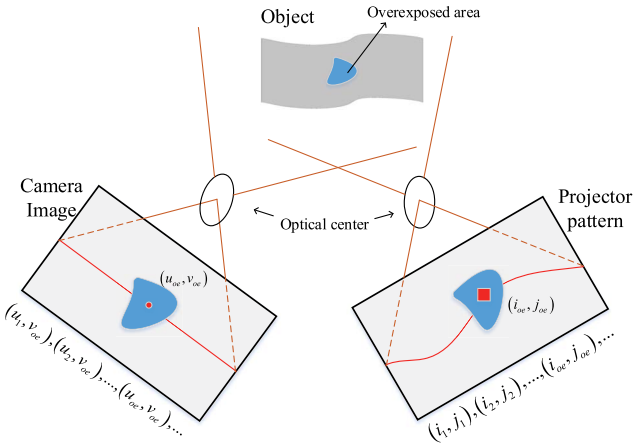

Fig. 2. Interpolation and error compensation. [Blue patches represent overexposed areas. Red point in the camera image represents overexposed point (u_{oe}, v_{oe}), while the red square in the projector pattern is the corresponding area around the overexposed point (i_{oe}, j_{oe}).]

the size of the overexposed area. Nevertheless, if there are some large overexposed areas, occlusions, shadows, or missing fringes, the corresponding square area may not contain the accurate corresponding pixel. The problem will be solved in the later iterations, in which the overexposed area is decreased with the modified projection image, and the estimation by interpolation is closer to the accurate corresponding pixel.

In the experiment of the paper, a equals seven and is able to work well. What is more, for different overexposed camera pixels, the corresponding square areas may cover part of the properly exposed area in the projection image and overlap each other. For the coverage, these can be discarded to ensure that properly exposed areas are not affected. For the overlapping, only the largest correction factor will be adopted for the same projector pixel, which will be introduced in Section 3.B.

B. Generating the Gray-Scale Correction Function

To reduce the number of iterations and to modify the projected image in the appropriate range, different overexposure conditions must be classified. The gray-scale correction function can be generated from the feedback of information captured by the camera. As the result of the four-step phase-shifting measurement, the projected image intensity can be represented as

$$I = A + B\cos\phi, \tag{1}$$

where A is the projected image offset, and B is the projected image amplitude.

Each pixel on the camera images has four intensity values I_1, I_2, I_3, and I_4, corresponding to four projection images of the four-step phase-shifting method that can be mathematically described as

$$\begin{aligned} I1 &= I'' + I'\cos\varphi, \\ I2 &= I'' + I'\cos\left(\varphi + \frac{\pi}{2}\right) = I'' + I'\sin\varphi, \\ I3 &= I'' + I'\cos(\varphi + \pi) = I'' - I'\cos\varphi, \\ I4 &= I'' + I'\cos\left(\varphi + \frac{3\pi}{2}\right) = I'' - I'\sin\varphi, \end{aligned} \tag{2}$$

where I' and I'' are constant coefficients during the measurement process for each camera pixel.

For convenience, the four intensity values are sorted from large to small and labeled as $I_{max}, I_{sec}, I_{thd}, I_{min}$, as shown in Fig. 3.

For an overexposed point, there is a rough classification to describe the degree of overexposure, using the number of intensity values that are overexposed for a pixel point. Overexposure conditions are divided into single-value overexposed (1-VOE), two-value overexposed (2-VOE), three-value overexposed (3-VOE), and four-value overexposed (4-VOE). For the surface area with low overexposure, only one or two intensity values may be overexposed, while for the surface area with higher overexposure, there may be three or even four intensity values overexposed.

To obtain the gray-scale correction function more accurately, an additional image is projected in the experiment. The gray value of the additional image should meet the following requirements: (1) The gray value is linearly related to other projected images; (2) the gray value is lower than other projected images; (3) the reflected image should avoid underexposure.

In order to satisfy the first requirement, the projected image intensity should be expressed as Eq. (3), where c is a constant. Then, to meet the second and third requirements, c should always be lower than $\cos\phi$ and should not be too low to avoid underexposure. Therefore, $c = -1.25$ is a good choice for the additional image intensity to meet the above requirements:

$$I_{padd} = A + cB. \tag{3}$$

According to the linear characteristic, the additional image intensity I_{add} captured by the camera is

$$I_{add} = I'' - 1.25I'. \tag{4}$$

Based on the above classification, the gray-scale correction function for different overexposure conditions is discussed as follows.

1. Single-Value Overexposed

For the pixels whose single intensity value is overexposed, there is only intensity value I_{max}, reaching the upper limit of intensity (i.e., saturating the camera image), while the intensity values I_{sec}, I_{thd}, and I_{min} are still accurate. Because the four-step phase-shifting method is used, there is a relationship among the four intensity values for those pixels with 1-VOE as

$$I_{max} + I_{min} = I_{sec} + I_{thd} = 2I''. \tag{5}$$

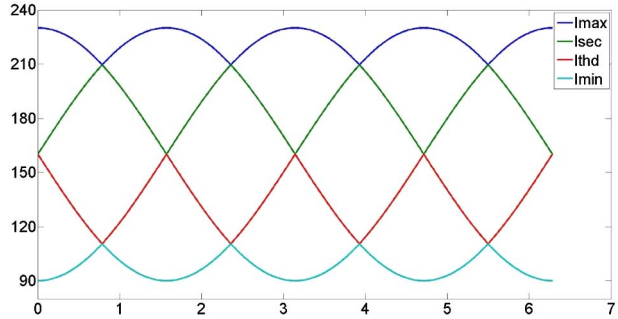

Fig. 3. Four intensity values of the camera pixel (sorted by size).

From Eq. (5), we obtain the undistorted maximum value I_{max} (e.g., greater than 255 for a 8 bit camera) by

$$I_{max} = I_{sec} + I_{thd} - I_{min}. \quad (6)$$

Because there is a linear relationship between the projection image intensity and camera image intensity, the correction factor K can be defined by dividing the undistorted maximum value I_{max} by the overexposure threshold as

$$K = \frac{I_{max}}{I_{oe}}, \quad (7)$$

where I_{oe} is the threshold for judging whether the captured image is overexposed. However, with the interference of the environment and equipment noise, the intensity value in the captured image is not unique but fluctuating, which leads to the phenomenon that there will be some properly exposed points without any change getting overexposed in the later iteration. Therefore, the threshold I_{oe} is set lower than 255 (which is the threshold of overexposed pixels without noise) and is concretely set at 250 in the experiment to reduce the influence of noise.

The gray-scale correction function can be determined by the correction factor K. In the experiment, the corrected projection image intensity can be obtained by dividing the corresponding projection image intensity by the correction coefficient,

$$I'_p = \frac{I_p}{K}, \quad (8)$$

where I'_p denotes the modified projection intensity, and I_p represents the projection intensity before modification.

According to the linear relationship between projection image intensity and camera image intensity, the modified projection image is projected again; the maximum intensity value of the original overexposed point is expected to be

$$I'_{max} = \frac{I_{max}}{K} = I_{oe}, \quad (9)$$

where I'_{max} denotes the maximum intensity value of the camera captured image after the modified images are projected. Therefore, I'_{max} is expected to be equal to I_{oe} and less than 255. The overexposure no longer exists, and the original overexposed area can be reconstructed.

2. Two-Value Overexposed

For pixels with two intensity values overexposed, there are intensity values I_{max} and I_{sec}, reaching the upper limit of intensity, while the intensity values I_{thd} and I_{min} are still properly exposed. To calculate the maximum intensity value I_{max} accurately, the intensity I_{add} of the additional image is adopted. The formula of maximum intensity and the additional intensity can be described as

$$I_{max} = I'' + I'\cos_{max} = I_{add} + 1.25I' + I'\cos_{max}, \quad (10)$$

where $\cos_{max}$ is the maximum value of the series $\{\cos(\varphi), \cos(\varphi + \frac{\pi}{2}), \cos(\varphi + \pi), \cos(\varphi + \frac{3\pi}{2})\}$, and φ is the projection initial phase corresponding to the camera pixels. Sort the four cosine values from large to small and $\{\cos_{max}, \cos_{sec}, \cos_{thd}, \cos_{min}\}$ is obtained. The relationship between I_{thd} and I_{add} is displayed as

$$I' = \frac{I_{thd} - I_{add}}{(1.25 + \cos_{thd})}. \quad (11)$$

From Eqs. (10) and (11), the undistorted maximum value I_{max} can be expressed as

$$I_{max} = I_{add} + \frac{1.25 + \cos_{max}}{1.25 + \cos_{thd}}(I_{thd} - I_{add}). \quad (12)$$

For an overexposed point, the intensity values I_{thd} and I_{add} can be obtained from the camera captured images directly, while the cosine values $\cos_{max}$ and $\cos_{thd}$ depend entirely on the projection initial phase φ, corresponding to the camera overexposed pixels. For a known projection image, the initial phase φ is determined by its projection pixel point coordinate (i_{oe}, j_{oe}) as

$$\varphi = \frac{i_{oe}}{T}2\pi, \quad (13)$$

where φ is the projection initial phase, and T is the period of the projected image. i_{oe} is the projector row coordinate of the overexposed pixel point, which can be obtained by the above method. Because of the fitting error, the phase value i_{oe} is used to substitute the phase of the surrounding estimation field.

The correction factor K is calculated similarly to the process of 1-VOE. Considering that there is intersection among the estimation field, the maximum value of the correction factor K in the estimation fields is chosen as the correction factor for the same overexposed point.

Therefore, for the points with 2-VOE, the capturing intensity of the camera is obtained first, and, then, the projection initial phase information of the overexposed points is estimated by the captured image of the camera. The undistorted maximum value I_{max} is calculated by combining the captured intensity and phase information. From Eq. (7), the correction factor K can be obtained.

3. Three-Value Overexposed

For the points with 3-VOE, there are intensity values I_{max}, I_{sec}, and I_{thd} reaching the upper limit of intensity, while the intensity values I_{min} and I_{add} are still valid. There is a relationship between I_{min} and I_{add} as

$$I_{min} - I_{add} = (1.25 + \cos_{min})I'. \quad (14)$$

Similarly, the undistorted maximum value I_{max} can be deduced as

$$I_{max} = I_{add} + \frac{1.25 + \cos_{max}}{1.25 + \cos_{min}}(I_{min} - I_{ad}). \quad (15)$$

For the pixels whose two intensity values are overexposed, the valid intensity values of I_{min} and I_{add} and the undistorted maximum value I_{max} can be calculated after the captured intensity. Then, the phase information and the correction factor can be obtained.

4. Four-Value Overexposed

For the condition that the four intensity values of the captured pixel all are distorted, it is impossible to estimate the maximum intensity value from the existing information. In this case, the maximum value of correction factor K of the surrounding field is adopted to substitute for the correction factor K of pixels with 4-VOE.

After modification and projection again, for the original 4-VOE point, there are the following three situations: (1) The pixel point is no longer overexposed and does not need more modification; (2) the pixel point is still overexposed, but the situation of overexposure has been improved to become one of the three kinds of overexposure introduced above, then, only one more iteration is required; (3) the pixel point is still 4-VOE. For the third case, the original minimum projection intensity is low. The minimum projection intensity is lower after an iteration, but it is still overexposed. The 4-VOE caused by low-intensity input indicates that the surface reflectivity of the object is too high, or there is reflected light shooting into the camera lens directly, which should be avoided in FPP. In the ordinary process of FPP 3D measurement, these situations should be avoided as much as possible, so the third case of 4-VOE is not discussed.

C. Phase Error Simulation

To better illustrate the necessity of overexposed modification, the phase calculated from the intensity values of the camera captured image is simulated. The phase calculation formula of four-step phase-shifting is expressed as

$$\varphi = \arctan\left(\frac{I_4 - I_2}{I_1 - I_3}\right), \tag{16}$$

where φ is the projection initial phase, and I_1, I_2, I_3, and I_4 are four intensity values of the captured images.

As the degree of overexposure can be described with the number of overexposed intensity values, there is a different error for a different number of overexposed intensity values. Simulation is carried out under different conditions, and the phase error is plotted in Fig. 4. Notice that it is unable to compute the phase of the pixel with 4-VOE, so the corresponding image is not plotted.

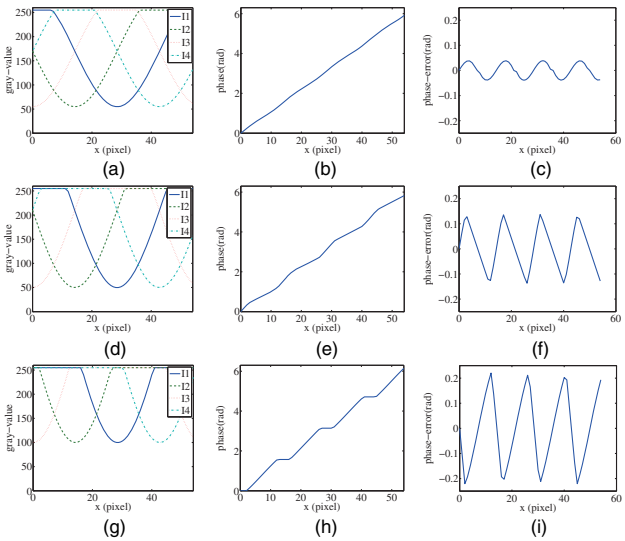

Fig. 4. Phase simulation of different degrees of overexposure: (a) intensity distribution of 1-VOE; (b) absolute phase of 1-VOE; (c) phase error of 1-VOE; (d) intensity distribution of 2-VOE; (e) absolute phase of 2-VOE; (f) phase error of 2-VOE; (g) intensity distribution of 3-VOE; (h) absolute phase of 3-VOE; (i) phase error of 3-VOE.

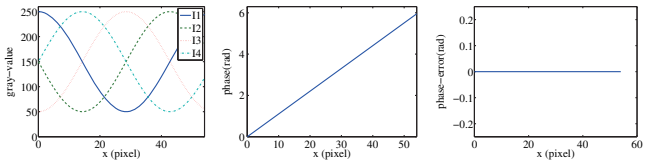

Fig. 5. Phase simulation after modification: (a) intensity distribution after modification; (b) absolute phase after modification; (c) phase error after modification.

From Fig. 4, the maximum phase errors are 0.04, 0.1, and 0.22 rad for 1-VOE, 2-VOE, and3-VOE. The phase error will be greater with the larger fluctuation of the phase for an overexposed object.

To reduce the phase error, the projection intensity of each pixel is adjusted dynamically to address overexposure point-by-point. Taking the 3-VOE as an example, the intensity distribution, the phase, and the phase error decoded by the modified camera images are shown in Fig. 5.

Comparing the simulation of the modified projection image with the unmodified image, the intensity of the captured image after modification is sinusoid, while the intensity of the initial image is distorted in most phase cases. There is no longer a point with a saturation intensity value with the modified image, and the absolute phase is a straight line with a phase error of nearly zero. Therefore, for the dynamic projection theory, we get a good decoded absolute phase without considering the influence of noise and defocusing, and the phase error is close to zero.

4. EXPERIMENT

Experiments were conducted to verify the validity of the dynamic projection theory. The USB-GO-5000M JAI camera and the Light Crafter 4500 digital light processing (DLP) projector are used in the experiment. The resolution of the projector is 912 × 1140 pixels, and the resolution of the camera is 2560 × 2048 pixels. The systems of the projector and camera were calibrated before the experiment.

A simple flat plate model is reconstructed first. There is a white area on the light gray plane; the flat model is shown in Fig. 6. There is a significant difference in reflectance between the white and gray areas. During the experiment, the white area is prone to overexposure due to the high reflectivity, which leads to a decoding error.

To obtain an accurate reconstructed result, the DLP intensity was manually adjusted to a lower level to prevent the surface from being overexposed. The result is shown in Figs. 7(a) and 7(d). Figure 7(a) is the 3D reconstruction, which may have some ripple errors due to too few steps with the four-step phase-shifting method. Figure 7(d) is the absolute phase information decoding from the intensity of the camera image. From Figs. 7(a) and 7(d), reconstructing the surface model perfectly requires corresponding phase information with no abrupt mutation.

Then, traditional FPP was used to reconstruct the surface; the result is shown in Figs. 7(b), 7(e), and 7(g). Figure 7(b) is the 3D reconstruction. Comparing the result in Figs. 7(a)

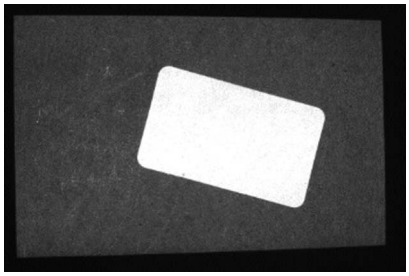

Fig. 6. Flat model.

and 7(b), it is obvious that the original light gray plane is reconstructed well, while the original white highlighted region is decoded badly, and the depth of the white region is corrugated severely and cannot stay flat. Figures 7(e) and 7(g) are the absolute phase information and phase error. Although the phase mutation in Fig. 7(e) is small compared to phase change along the x axis, the phase error in Fig. 7(g) shows that there is an abrupt mutation in the white region.

Finally, the dynamic projection theory was used to measure the plate model. In the experiment, the number of overexposed points decreased from the initial 270,000 to 6000 after an iteration; the experimental result is shown in Figs. 7(c), 7(f), and 7(h). Figure 7(c) is the point cloud of the reconstructed 3D surface. Comparing Figs. 7(c) and 7(b) shows that the dynamic projection theory is much better for white overexposure region reconstruction, and the decoding problem due to overexposure is eliminated. Figures 7(f) and 7(h) are the corresponding absolute phase map and phase error. As seen from Fig. 7(h), the abrupt mutation has been decreased, and only a little phase error remains.

A statue was then reconstructed. As shown in Fig. 8, due to the difference in angle, position, and surface reflectivity, the

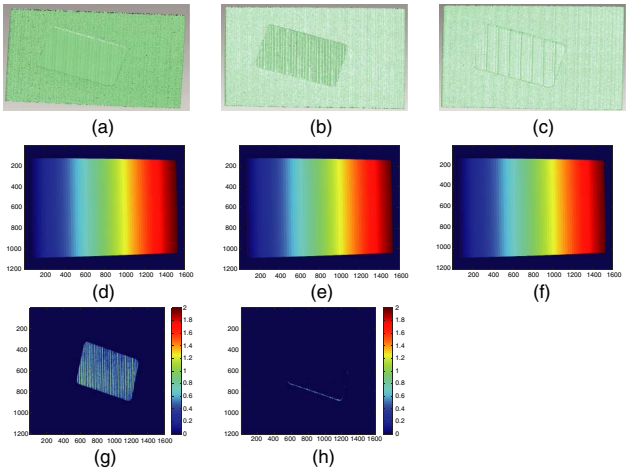

Fig. 7. Measurement result of a plate object: (a) 3D reconstruction without overexposure; (b) 3D reconstruction with the traditional method; (c) 3D reconstruction with dynamic projection theory; (d) phase map without overexposure; (e) phase map with the traditional method; (f) phase map with dynamic projection theory; (g) phase error with the traditional method; (h) phase error with the dynamic projection theory.

Fig. 8. Head statue model.

intensity values of different pixels of the image captured by the camera are different. Thus, overexposure is prone to occur in some areas.

Similarly, as shown in Figs. 9(a) and 9(d), multiple measurements for properly exposed areas are adopted to obtain accurate 3D information and complete absolute phase information. Figure 9(d) shows that the decoded phase information perfectly reflects the physical contours in the camera without overexposure.

Because there is no prior knowledge of the surface of the target object surface, the local area may be overexposed with the same projection brightness. In this case, the result is shown in Figs. 9(b), 9(e), and 9(g), where the target surface is reconstructed with the traditional method. Figure 9(b) is the point cloud of 3D reconstruction, including 250,000 overexposed points, so there is a large error. As we can see in Fig. 9(b), part

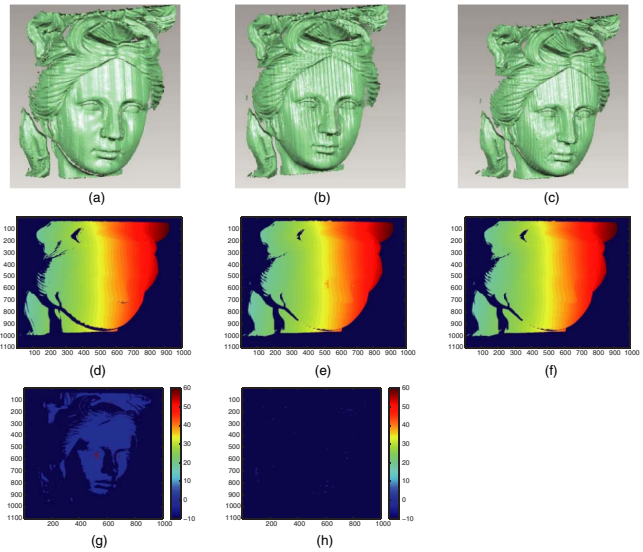

Fig. 9. Result of statue model. (a) 3D reconstruction without overexposure; (b) 3D reconstruction with the traditional method; (c) 3D reconstruction with dynamic projection theory; (d) phase map without overexposure; (e) phase map with the traditional method; (f) phase map with dynamic projection theory; (g) phase error with the traditional method; (h) phase error with dynamic projection theory.

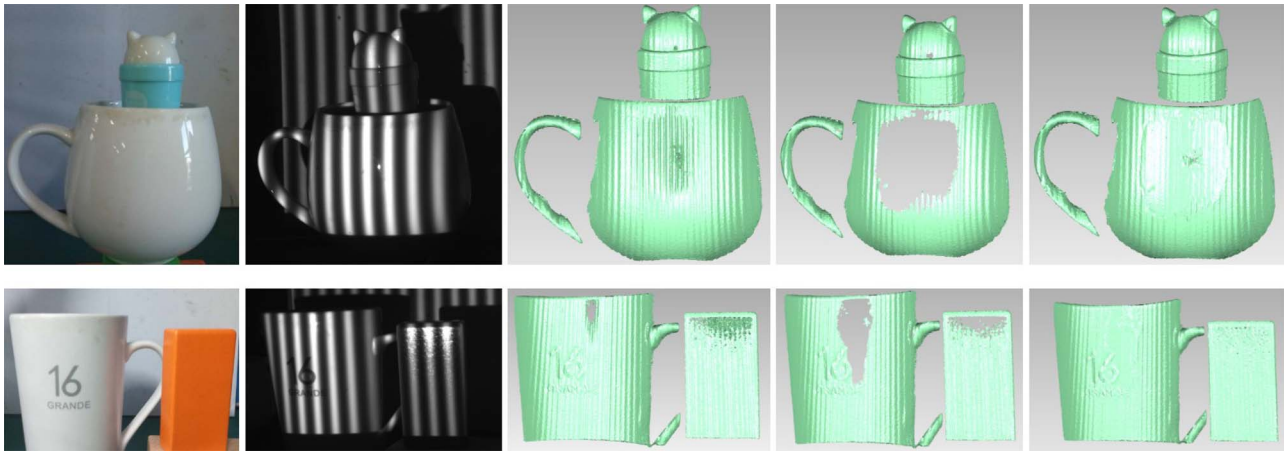

Fig. 10. Reconstruction of objects with different materials/reflectivity index surfaces. The first row, a ceramic cup and a plastic toy; the second row, a white cup and an orange block; the left-most column, the objects; the second column, the objects under fringe projection; the third column, 3D reconstruction with the traditional method; the fourth column, 3D reconstruction except overexposed areas; the right-most column, 3D reconstruction with the dynamic projection theory.

of the 3D reconstruction is incorrectly decoded. Figure 9(e) is the corresponding absolute phase map. It is found from the phase map that an abrupt mutation of phase exists, resulting in a final error in reconstruction. Figure 9(g) is the phase error map with the traditional method (notice, to show the detail, the phase error of the background is set from 0 to −10). It is obvious that there is phase error over the surface of the statue, and points with more severe overexposure are decoded less effectively.

The dynamic projection method is then used to measure the statue surface based on FPP; the 3D reconstruction and absolute phase map are obtained as Figs. 9(c) and 9(f) after two iterations. Compared with the traditional method, the number of overexposed points is decreased from 250,000 to approximately 3000. The camera image intensity is not decoded incorrectly because of intensity distortion. Comparing Fig. 9(c) with Fig. 9(b), the complete surface of the target object is reconstructed by dynamic projection theory, and the reconstruction result is improved so that there is no large deviation, as in Fig. 9(b). However, comparing Fig. 9(c) with Fig. 9(a), in the details, the results in Fig. 9(c) are not as smooth as in Fig. 9(a) because of uneven distribution of the intensity and defocusing. Defocusing can be reduced by adjusting the distance to focus. Comparing Figs. 9(f) and 9(e), the phase map is smooth enough after two iterations, and no obvious abrupt mutation exists, which shows that the dynamic projection theory is effective for addressing the problem of overexposure. Figure 9(h) is the phase error with dynamic projection theory. Compared with Fig. 9(g), only a little phase error remained, and the result is satisfactory.

To further verify the validity of the dynamic projection theory, additional objects with different materials and reflectivity index surfaces are reconstructed. The experiment objects are shown in Fig. 10. In the first row, a ceramic cup and a plastic cat toy with a shiny surface are reconstructed, while a white cup and an orange block are chosen in the second row. The reconstruction results are shown in the right-most column. Almost all objects, including overexposure areas, can be well reconstructed, which demonstrate that the dynamic projection theory is valid for overexposure in 3D reconstruction.

However, as stated in Section 3.B.4, the dynamic projection theory cannot deal with the situation of specular reflection, in which the captured image is always overexposed with a little light. As a result, for the reconstruction, there are some blemishes in the center of the shiny cup and the top of the orange block affected by specular reflection, which should be studied in the future work.

5. CONCLUSION

In this paper, a dynamic projection theory for FPP is proposed, which can measure complete 3D information of an object without any change to the setup. Dynamic projection theory does not require additional information and can measure complex reflective objects with simple operations. The proposed theory can modify the projection image according to the feedback of information concerning overexposed points. The intensity of the projection image pixel corresponding to the overexposed point is reduced to bring the camera intensity down to a measurable range. Simulation shows the necessity for reducing the intensity of the overexposure region in the projection image for accurate phase recovery.

Experiments on the objects with different material and reflectivity index surfaces demonstrated that the dynamic projection theory is effective in measuring overexposed areas and broadens the range of FPP. Because the dynamic projection theory only requires 1–2 iterations (in most cases one iteration is enough), the dynamic projection theory for FPP is very efficient. However, there are some shortcomings in dynamic projection theory. When measuring out-of-focus objects, the error in a region with an abrupt mutation will increase due to the inconsistent intensity distribution, and our future research will address this limitation.

Funding. National Natural Science Foundation of China (NSFC) (U1613205, 51675291); State Key Laboratory of China (SKLT2015B10); Basic Research Program of Shenzhen (JCYJ20160229123030978).

REFERENCES

1. S. Kurada and C. Bradley, "A review of machine vision sensors for tool condition monitoring," Comput. Ind. **34**, 55–72 (1997).
2. J. Kofman and K. Borribanbunpotkat, "Hand-held 3D scanner for surface-shape measurement without sensor pose tracking or surface markers: a compact hand-held 3D scanner simultaneously projecting multiple light lines is presented, enabling 3D surface-shape measurement without requiring sensor tracking or surface markers," Virtual Phys. Prototyping **9**, 81–95 (2014).
3. L. Zhang, Q. Ye, W. Yang, and J. Jiao, "Weld line detection and tracking via spatial-temporal cascaded hidden Markov models and cross structured light," IEEE Trans. Instrum. Meas. **63**, 742–753 (2014).
4. B. D. Lucas and T. Kanade, "An iterative image registration technique with an application to stereo vision," in *International Joint Conference on Artificial Intelligence* (1981), pp. 674–679.
5. Z. Liu, Y. Yin, Q. Wu, X. Li, and G. Zhang, "On-site calibration method for outdoor binocular stereo vision sensors," Opt. Lasers Eng. **86**, 75–82 (2016).
6. F. Xi, Y. Liu, and H. Y. Feng, "Error compensation for three-dimensional line laser scanning data," Int. J. Adv. Manuf. Technol. **18**, 211–216 (2001).
7. Q. Sun, J. Chen, and C. Li, "A robust method to extract a laser stripe centre based on grey level moment," Opt. Lasers Eng. **67**, 122–127 (2015).
8. Z. Wei, M. Shao, G. Zhang, and Y. Wang, "Parallel-based calibration method for line-structured light vision sensor," Opt. Eng. **53**, 033101 (2014).
9. R. J. Valkenburg and A. M. Mcivor, "Accurate 3D measurement using a structured light system," Image Vis. Comput. **16**, 99–110 (1998).
10. P. Wang, J. Wang, J. Xu, Y. Guan, G. Zhang, and K. Chen, "Calibration method for a large-scale structured light measurement system," Appl. Opt. **56**, 3995–4002 (2017).
11. F. Deng, C. Liu, W. Sze, J. Deng, K. S. M. Fung, and E. Y. Lam, "An inspect measurement system for moving objects," IEEE Trans. Instrum. Meas. **64**, 63–74 (2015).
12. E. Lilienblum and A. Al-Hamadi, "A structured light approach for 3-D surface reconstruction with a stereo line-scan system," IEEE Trans. Instrum. Meas. **64**, 1258–1266 (2015).
13. G. Sansoni, M. Carocci, and R. Rodella, "Calibration and performance evaluation of a 3-D imaging sensor based on the projection of structured light," IEEE Trans. Instrum. Meas. **49**, 628–636 (2000).
14. S. Zhang and P. S. Huang, "Novel method for structured light system calibration," Opt. Eng. **45**, 083601 (2006).
15. R. Porras-Aguilar and K. Falaggis, "Absolute phase recovery in structured light illumination systems: sinusoidal vs. intensity discrete patterns," Opt. Lasers Eng. **84**, 111–119 (2016).
16. D. Scharstein and R. Szeliski, "High-accuracy stereo depth maps using structured light," in *IEEE Computer Society Conference on Computer Vision and Pattern Recognition* (2003), Vol. **1**, pp. 195–202.
17. K. L. Boyer and A. C. Kak, "Color-encoded structured light for rapid active ranging," IEEE Trans. Pattern Anal. Mach. Intell. **PAMI**-9, 14–28 (1987).
18. J. Salvi, J. Pagés, and J. Batlle, "Pattern codification strategies in structured light systems," Pattern Recogn. **37**, 827–849 (2004).
19. A. Subramanian, L. G. Hassebrook, and P. Pai, "Optimized 3-D recovery from 2-D images using sine-wave-structured light illumination," Visual Inf. Process. **1705**, 89–99 (1992).
20. J. Salvi, S. Fernandez, T. Pribanic, and X. Llado, "A state of the art in structured light patterns for surface profilometry," Pattern Recogn. **43**, 2666–2680 (2010).
21. C. Zhang, J. Xu, N. Xi, J. Zhao, and Q. Shi, "A robust surface coding method for optically challenging objects using structured light," IEEE Trans. Autom. Sci. Eng. **11**, 775–788 (2014).
22. J. Clark, E. Trucco, and L. B. Wolff, "Using light polarization in laser scanning," Image Vis. Comput. **15**, 107–117 (1997).
23. S. Zhang and S.-T. Yau, "High dynamic range scanning technique," Opt. Eng. **48**, 033604 (2009).
24. M. Shao, Z. Wei, M. Hu, and G. Zhang, "Correction method for line extraction in vision measurement," PLoS ONE **10**, e0127068 (2015).
25. B. Chen and S. Zhang, "High-quality 3D shape measurement using saturated fringe patterns," Opt. Lasers Eng. **87**, 83–89 (2016).
26. B. Budianto and D. P. K. Lun, "Inpainting for fringe projection profilometry based on geometrically guided iterative regularization," IEEE Trans. Image Process. **24**, 5531–5542 (2015).
27. H. Wang, Q. Kemao, and S. H. Soon, "Valid point detection in fringe projection profilometry," Opt. Express **23**, 7535–7549 (2015).
28. C. Jiang, T. Bell, and S. Zhang, "High dynamic range real-time 3D shape measurement," Opt. Express **24**, 7337–7346 (2016).
29. M. Gupta, A. Agrawal, A. Veeraraghavan, and S. G. Narasimhan, "A practical approach to 3D scanning in the presence of interreflections, subsurface scattering and defocus," Int. J. Comput. Vis. **102**, 33–55 (2013).
30. S. K. Nayar and M. Gupta, "Diffuse structured light," in *IEEE International Conference on Computational Photography* (2012), pp. 1–11.
31. D. Li and J. Kofman, "Adaptive fringe-pattern projection for image saturation avoidance in 3D surface-shape measurement," Opt. Express **22**, 9887–9901 (2014).
32. B. Budianto and D. P. K. Lun, "Robust fringe projection profilometry via sparse representation," IEEE Trans. Image Process. **25**, 1726–1739 (2016).
33. P. F. Almoro, G. Pedrini, P. N. Gundu, W. Osten, and S. G. Hanson, "Enhanced wavefront reconstruction by random phase modulation with a phase diffuser," Opt. Lasers Eng. **49**, 252–257 (2011).